Steady state and relaxation dynamics of run-and-tumble particles in contact with a heat bath

R. K. Singh* and Oded Farago†
Department of Biomedical Engineering, Ben-Gurion University of the Negev, Be'er Sheva 85105, Israel

(Received 1 April 2025; revised 12 May 2025; accepted 2 June 2025; published 23 June 2025)

We study the relaxation dynamics of a run and tumble particle (RTP) in a one-dimensional piecewise linear potential $U(x) = b|x|$, from delta-function initial conditions at $x = 0$ to steady state. In addition to experiencing active telegraphic noise, the particle is in contact with a heat bath at temperature T that applies white thermal noise. We find that the position distribution of the RTP is described by a sum of two distributions ("modes"), each of which of the form $P(x, t \to \infty) \sim e^{-\lambda_i |x|}$ $(i = 1, 2)$ at steady state. The two modes are dynamically coupled: At very short times $(t \to 0)$, each mode stores half of the probability, and exhibits thermal diffusive spreading with a Gaussian profile. With progressing time and evolution toward steady state, the partition of probability between the modes becomes increasingly uneven, and, depending on the model parameters, the mode with the smaller value of λ_i may carry an overwhelming majority of the probability. Moreover, we identify that the characteristic relaxation time of each mode is $\tau_i = (\lambda_i^2 T)^{-1}$, which implies that the minority mode also relaxes much faster than the dominant one. A more detailed analysis reveals that τ_i is characteristic of the mode relaxation only close to the origin at the core of the distribution, while farther away it increases linearly with $|x|$ as if a relaxation front is propagating at constant speed $v_i^* = 2\sqrt{T/\tau_i}$ in the system. The rate of nonequilibrium entropy production can be related to the two-mode splitting of the probability distribution and be expressed in terms of their correlation lengths λ_i and their contributions to the steady-state distribution.

DOI: 10.1103/c51r-fmgw

I. INTRODUCTION

Active particles use energy from the environment to fuel their motion which is inherently out of equilibrium [1–5]. Activity dominates the dynamics of, e.g., molecular motors [6–9], transport within cells [10–12], and bird flocking [13,14], to mention a few. The ubiquity of active particles has prompted investigations of their properties also from the perspective of applications, like designing phoretic swimmers [15], acoustic and harmonic trapping of active systems [16,17], and engineering self-propelled robots [18].

Bacterial dynamics in fluids constitutes yet another example of nonequilibrium active motion. Movement of bacteria in fluids is characterized by phases of runs in which the bacteria travels in straight lines, separated by tumbling events marking the directional changes [19–24]. These dynamical aspects of bacterial motion have been explored within the model of run and tumble particles (RTPs), which is one of the more extensively studied models in nonequilibrium statistical physics [25–34]. In the simplest setting, an RTP moves with a fixed speed, undergoing random tumbling events at a constant rate. The resulting motion is described by the telegrapher's equation [35–37], which unlike the diffusion equation for Brownian motion is second order in both space and time. This leads to many interesting physical properties, notable being the motion confined within a spatiotemporal light cone [38]. Nevertheless, at times much larger than the mean tumbling time and in free space, an RTP exhibits diffusive behavior similar to a Brownian particle.

The differences in the dynamical properties of the RTP and a Brownian particle become apparent when their respective motions are subject to confinement by an external potential. Generally speaking, the steady state of an RTP in a confining potential is non-Boltzmannian [39–41]. Moreover, if the associated restoring force exceeds the active force such as in the case of a harmonic potential, the steady state of the RTP is defined only over a finite support [39,42]. This is in sharp contrast to a Brownian motion in the same potential, for which the steady state has an infinite support [43]. The intrinsic activity of RTPs also renders their first passage properties complex and counter to the intuition based on the first passage properties of Brownian particles [44,45].

In most cases of practical interest, the motion of RTPs often takes place at a finite temperature [46,47]. In the literature, however, most studies focus on RTP dynamics under the influence of a telegraphic (dichotomous) noise only, and the influence of an additional white thermal noise has been relatively less explored [48–55]. The significant differences between the statistical behavior of RTPs and Brownian particles makes it imperative to study the dynamical properties of RTPs that are also subject to both types of noises. The prime question is whether the coupling to a heat bath modifies the dynamical properties in a nontrivial way, or just increases the fluctuations in position due to the additional thermal noise. This question is particularly relevant for understanding physical systems such as bacteria, whose motion can be effectively described by the RTP model, but which, in reality, operate at finite temperatures. A predictable consequence of introducing

*Contact author: rksinghmp@gmail.com
†Contact author: ofarago@bgu.ac.il

white thermal noise into the model is that the particle's motion will no longer be restricted to a finite spatial domain. In this paper, we present a rare example where (i) the steady-state distribution (SSD) can be computed exactly, and (ii) the dynamical evolution toward the steady state can be analyzed in Laplace space and approximated in the time domain. Our findings highlight that the interplay between active and thermal noise can lead to intricate dynamical behavior.

The dynamics of an RTP in a one-dimensional potential $U(x)$ and in contact with a heat bath is described by the Langevin equation

$$\frac{dx}{dt} = f[x(t)] + \sigma(t) + \eta(t), \tag{1}$$

where $f(x) = -dU(x)/dx$ is the force acting on the particle, while $\sigma(t)$ and $\eta(t)$ are active telegraphic (dichotomous) and thermal noises, respectively. Note that we set the mobility μ to unity in Eq. (1), so that the forces on the r.h.s. of Eq. (1) are expressed in units of velocity (and the conversion back to units of force is done via force $= \mu^{-1} \times$ velocity). The active noise switches between the two values $\sigma(t) = \pm v_0$ at a fixed rate r, i.e., the time between consecutive switches is drawn from an exponential distribution with mean running time r^{-1}. The thermal noise is a white Gaussian noise with zero mean and correlation $\langle \eta(t)\eta(s)\rangle = 2T\delta(t-s)$, where T denotes the temperature of the heat bath. Here we adopt the common convention of setting Boltzmann constant k_B to unity. In this notation, diffusion coefficient D is expressed in units of the corresponding temperature, as defined by the Einstein relation $D = \mu k_B T$. Interestingly, Langevin Eq. (1) describing the motion of an RTP in contact with a heat bath also describes the motion of a Brownian particle in a dichotomously fluctuating potential $U(x) \pm v_0(t)x$. The latter problem was considered in a 1993 paper by Bier and Astumian (BA) [56] who studied the mean escape time from a fluctuating potential well. Here we exploit the equivalence between the two problems to derive expressions for the SSD of an RTP moving in an external potential and subject to thermal noise. We extend the BA approach to study also the corresponding time-dependent Fokker-Planck (FP) equation, analyze the relaxation of an initial delta-function distribution to the SSD, and unravel the interplay between the active and thermal noises. As in Ref. [56], we consider a piecewise linear potential of the form $U(x) = b|x|$, which is also relevant to the study of active particle sedimentation, where the SSD is determined by the solution of the Mathieu equation [57]. Within the context of the RTP model, the linear potential is appealing for at least two reasons. First, it allows for an exact analytical solution, namely, a derivation of a closed-form expression of the SSD, because the total force acting on the particle takes only two values: $(v_0 - b)$ when moving outward of the origin, and $(v_0 + b)$ when moving toward the origin. Second, unlike a harmonic potential [and more generally, any potential of the form $U(x) \sim |x|^a$ with $a > 1$], the piecewise linear potential has infinite support even in the absence of thermal noise, as long as $v_0 > b$. In fact, the SSD of such an RTP has a form which is similar to the equilibrium Boltzmann distribution [39,58]

$$P(x) \sim e^{-b|x|/T^*}, \tag{2}$$

with $T^* = (v_0^2 - b^2)/2r$. However, as will be shown below, the SSD of a particle following Langevin Eq. (1) does *not* have the form of Eq. (2) with temperature $T + T^*$, but rather follows a double exponential form. A single exponential form is obtained only in the limit when both $v_0 \to \infty$ and $r \to \infty$ such that the ratio $T_{\rm ac} = v_0^2/2r$ is fixed. In this limit, the active noise approaches a white Gaussian noise with mean zero and correlation $\langle \sigma(t)\sigma(s)\rangle = 2T_{ac}\delta(t-s)$, where $T_{\rm ac}$ is the active "temperature" (or the associated diffusion coefficient of the active noise; see the comment above about the correspondence between temperature and diffusion coefficient). Indeed, for a flat potential ($b = 0$), $T_{\rm ac}$ is the large-time diffusion coefficient of an RTP not coupled to a heat bath for any value of v_0 and r.

The paper is organized as follows: In Sec. II we study the long-time behavior of the distribution, $P(x,t)$, and derive the expression for the SSD, $P(x)$. In the following Sec. III we obtain the expression for the temporal evolution of the position distribution in Laplace space. An exact inversion of the function from Laplace space to the time domain is not possible. A closed-form analytical approximation is derived in Sec. IV, where we also present Langevin dynamics simulation results to analyze the relaxation dynamics to steady state. In Sec. V we briefly discuss and rate of entropy production at steady state. We summarize and discuss our main findings in Sec. VI

II. STEADY STATE OF THE RTP

Let $p_\pm(x,t)$ denote the distributions of the RTP to be at location x at time t with $\sigma(t) = \pm v_0$. Then the evolution of the distributions can be described by the set of coupled FP equations [43,59]:

$$\partial_t p_+(x,t) = -\partial_x[(f(x) + v_0)p_+(x,t)] - r p_+(x,t) + r p_-(x,t) + T\partial_{xx}p_+(x,t), \tag{3a}$$

$$\partial_t p_-(x,t) = -\partial_x[(f(x) - v_0)p_-(x,t)] + r p_+(x,t) - r p_-(x,t) + T\partial_{xx}p_-(x,t). \tag{3b}$$

The respective SSDs, $p_\pm(x)$, are obtained by solving the set of ordinary differential equations:

$$0 = -\frac{d}{dx}[(f(x) + v_0)p_+(x)] - r p_+(x) + r p_-(x) + T\frac{d^2}{dx^2}p_+(x), \tag{4a}$$

$$0 = -\frac{d}{dx}[(f(x) - v_0)p_-(x)] + r p_+(x) - r p_-(x) + T\frac{d^2}{dx^2}p_-(x). \tag{4b}$$

Symmetry of the problem implies that the above set of differential equations only needs to be solved in the region $x \geqslant 0$ and the solution for the region $x \leqslant 0$ follows by symmetry, $p_\pm(-x) = p_\mp(x)$. Furthermore, the SSD $P(x) = p_+(x) + p_-(x)$.

Let us now focus on the region $x \geqslant 0$, which implies that $f(x) = -b$. Following [56], we define

$$P_0(x) = p_+(x) + p_-(x), \tag{5a}$$

$$P_1(x) = \frac{dP_0}{dx}, \tag{5b}$$

$$D_0(x) = p_+(x) - p_-(x), \tag{5c}$$

$$D_1(x) = \frac{dD_0}{dx}, \tag{5d}$$

where $P_0(x) = P(x)$ is the SSD of the RTP. Using these definitions, we can write the set of Eqs. (4), in the following form:

$$\frac{d}{dx}P_0 = P_1,$$
$$\frac{d}{dx}\begin{pmatrix} P_1 \\ D_0 \\ D_1 \end{pmatrix} = \underbrace{\begin{pmatrix} -\frac{b}{T} & 0 & \frac{v_0}{T} \\ 0 & 0 & 1 \\ \frac{v_0}{T} & \frac{2r}{T} & -\frac{b}{T} \end{pmatrix}}_{M_3} \begin{pmatrix} P_1 \\ D_0 \\ D_1 \end{pmatrix}. \tag{6}$$

The structure of the above equations implies that the solution $(P_1\, D_0\, D_1)^\top$, where $\top$ denotes transpose, is determined by the eigenvalues of the matrix M_3, with the eigenvalues $\lambda_k \in \mathbb{R}\ \forall\, k = 1, 2, 3$ as the absence of any boundaries forbids oscillatory solutions. Furthermore

$$\mathrm{tr}\, M_3 = -\frac{2b}{T} < 0, \tag{7a}$$

$$\det M_3 = \frac{2rb}{T^2} > 0, \tag{7b}$$

with "tr" and "det" representing, respectively, the trace and determinant of the matrix M_3. This implies that two of the eigenvalues are negative and one is positive. The eigenvalues are determined by the solution of the equation $\det(M_3 - \lambda \mathbb{I}_3) = 0$, where $\mathbb{I}_3$ is the 3×3 identity matrix. The solution of the resulting cubic equation

$$\lambda^3 + \frac{2b}{T}\lambda^2 - \left(\frac{v_0^2}{T^2} + \frac{2r}{T} - \frac{b^2}{T^2}\right)\lambda - \frac{2rb}{T^2} = 0 \tag{8}$$

is well known [60,61]:

$$\lambda_k = -\frac{2b}{3T} + 2\sqrt{-\frac{q_1}{3}}\cos\left[\frac{1}{3}\cos^{-1}\left(\frac{3q_2}{2q_1}\sqrt{-\frac{3}{q_1}}\right) - \frac{2\pi k}{3}\right], \tag{9}$$

for $k = 0, 1, 2$, with $q_1 = -\frac{v_0^2}{T^2} - \frac{b^2}{3T^2} - \frac{2r}{T}$ and $q_2 = \frac{2bv_0^2}{3T^3} - \frac{2br}{3T^2} - \frac{2b^3}{27T^3}$. Among the three eigenvalues, we only choose the ones which are negative, as inclusion of the positive eigenvalue would lead to diverging solutions at large x (recall that we solve for $x \geqslant 0$).

Let λ_1 and λ_2 be the *absolute values* of two negative eigenvalues of the matrix M_3, then

$$P_1(x) = -A_1 e^{-\lambda_1 x} - A_2 e^{-\lambda_2 x}, \tag{10a}$$

$$D_0(x) = \frac{b - \lambda_1 T}{v_0 \lambda_1} A_1 e^{-\lambda_1 x} + \frac{b - \lambda_2 T}{v_0 \lambda_2} A_2 e^{-\lambda_2 x}, \tag{10b}$$

$$D_1(x) = -\frac{b - \lambda_1 T}{v_0} A_1 e^{-\lambda_1 x} - \frac{b - \lambda_2 T}{v_0} A_2 e^{-\lambda_2 x}. \tag{10c}$$

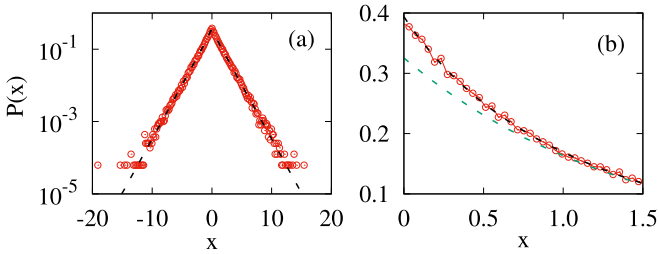

FIG. 1. (a) The SSD, $P(x)$, of the RTP obtained from Langevin dynamics simulations (red circles) and the analytical result in Eq. (11) (black dashed line). All the model parameters are set to unity: $r = 1$, $v_0 = 1$, $b = 1$, and $T = 1$, for which we have (see details in the text) $\lambda_1 \approx 0.69$, $\lambda_2 \approx 2.48$, $A_1/\lambda_1 \approx 0.32$, and $A_2/\lambda_2 \approx 0.07$. (b) Enlargement of the central region in (a). The green dashed lines depicts the large $|x|$ asymptotic Laplace distribution $\frac{A_1}{\lambda_1} e^{-\lambda_1 |x|}$. Langevin dynamics simulations were conduced with the Euler integration method with time step $dt = 4 \times 10^{-3}$ and are based on 10^6 trajectories.

Because $\frac{d}{dx}P_0 = P_1$, and because of the symmetry $P_0(x) = P_0(-x)$, we find that the SSD is given by

$$P(x) = P_0(x) = \frac{A_1}{\lambda_1} e^{-\lambda_1 |x|} + \frac{A_2}{\lambda_2} e^{-\lambda_2 |x|}. \tag{11}$$

The coefficients A_1 and A_2 can be found from the requirement that $D_0(0) = 0$, which follows from the symmetry of the system $[p_+(0) = p_-(0)]$, in conjunction with the fact that the SSD is normalized, that is, $\int_{-\infty}^{\infty} dx\, P_0(x) = 1$, yielding

$$\frac{1}{A_1} = 2\left(\frac{1}{\lambda_1^2} - \frac{1}{\lambda_1 \lambda_2}\frac{b - \lambda_1 T}{b - \lambda_2 T}\right), \tag{12a}$$

$$\frac{1}{A_2} = 2\left(\frac{1}{\lambda_2^2} - \frac{1}{\lambda_1 \lambda_2}\frac{b - \lambda_2 T}{b - \lambda_1 T}\right). \tag{12b}$$

Notice that A_1, A_2, λ_1 and λ_2 are related by the normaliuzation condition of the total SSD:

$$\frac{A_1}{\lambda_1^2} + \frac{A_2}{\lambda_2^2} = \frac{1}{2}. \tag{13}$$

The SSD defined by Eqs. (11) and (12), is a normalized linear combination of two Laplace distributions with distinct length scales. This form seems reasonable considering that it represents the SSD of a particle subjected to two noise sources, thermal and active, which individually lead to steady-state single-scale Laplace distributions. However, the two-noise SSD is not merely a linear combination of the one-noise SSDs: The inverse length scales λ_1 and λ_2 are related to the model parameters characterizing the two noise sources via an intricate relationship expressed by Eq. (9). Figure 1 shows Langevin dynamics simulations results corresponding to the case when all the model parameters are set to unity: $r = 1$, $v_0 = 1$, $b = 1$, and $T = 1$. For this set of model parameters, the two eigenvalues are $\lambda_1 \approx 0.69$ and $\lambda_2 \approx 2.48$ with the coefficients $A_1/\lambda_1 \approx 0.32$ and $A_2/\lambda_2 \approx 0.07$, i.e., $A_1 \approx 0.22$ and $A_2 \approx 0.17$. For comparison, the inverse length scales corresponding to Brownian and RTP without thermal contact

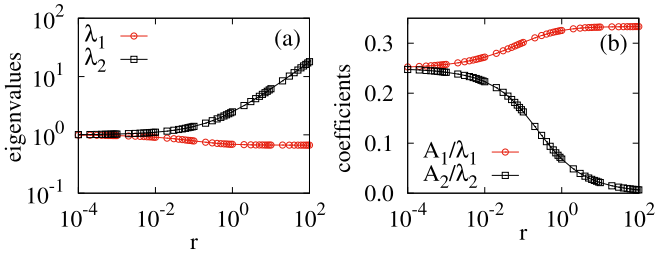

FIG. 2. (a) The eigenvalues and (b) the normalizations coefficients defining of the SSD, as a function of the tumbling rate r. The model parameter are set to $b = 1$, $T = 1$, and $T_{\rm ac} = v_0^2/2r = 1/2$.

dynamics would be, respectively, $\lambda_{\rm Br} = b/T = 1$, and $\lambda_{\rm RTP} = b/T^* = 2br/(v_0^2 - b^2) \to \infty$ (which is a reminder that in the absence of coupling to a heat bath, the RTP moves only when $v_0 > b$ [39,58]). Figure 1(a) reveals excellent agreement between the simulations results (red circles) and the SSD given by Eqs. (11) and (12) (dashed line). Figure 1(b) shows an enlargement of the central region of the SSD. The green dashed line shows the Laplace distribution $\frac{A_1}{\lambda_1} e^{-\lambda_1 |x|}$, which dominates the SSD at large $|x|$. The deviations, on length scales not much larger than $\lambda_2^{-1} \sim 0.40$, between the SSD and the asymptotic form are clearly visible.

As mentioned above, in the absence of one of the noises, the SSD takes the form of a single-exponential Laplace distribution. Apart from these two particular cases, there is one additional case resulting in a Laplace SSD, which is the thermal limit of the active noise obtained taking the limits $v_0 \to \infty$, $r \to \infty$ such that the ratio $v_0^2/2r = T_{\rm ac}$. In this limit, the particle is essentially moving under the influence of two independent thermal noises, which is equivalent to Brownian motion with $\lambda = b/(T + T_{\rm ac})$. Figure 2(a) shows the dependence of the two eigenvalues [negative solutions of Eq. (9)] on the rate of the active noise r, for $b = 1$, $T = 1$, and $T_{\rm ac} = 1/2$. The smaller λ_1 varies smoothly from $\lambda_1 = b/T = 1$ for $r = 0$ (no active noise) to $\lambda_1 = b/(T + T_{\rm ac}) = 2/3$, while the larger λ_2 increases monotonically with r, implying that the influence of the second exponential corresponding to the smaller length scale $1/\lambda_2$ becomes limited to the vicinity of the origin. Moreover, Fig. 2(b), which shows the amplitudes of the two terms in the SSD, demonstrates that increasing r leads to rapid reduction in the amplitude A_2/λ_2. For $r \to 0$, we have $\lambda_1, \lambda_2 \to 1$, and the corresponding normalizations are $A_1/\lambda_1 = A_2/\lambda_2 = 1/4$. When $r \to \infty$ the second exponential becomes irrelevant, and $A_1/\lambda_1 \to \lambda_1/2 = 1/3$.

As the properties of the steady state of the RTP are understood, a naturally arising question is how does the RTP relax to its steady state given the information about its initial configuration? We proceed to answer this question in the next section.

III. TIME-DEPENDENT SOLUTION

We now return to the set of Eqs. (3) and assume that at $t = 0$, the particle is located at the origin with equal probability to move to the right or left, i.e., $p_\pm(x, 0) = \frac{1}{2}\delta(x)$. Transforming Eqs. (3) in Laplace space gives

$$s\tilde{p}_+(x,s) - \tfrac{1}{2}\delta(x) = -\partial_x[(f(x) + v_0)\tilde{p}_+(x,s)] - r\tilde{p}_+(x,s) + r\tilde{p}_-(x,s) + T\,\partial_{xx}\tilde{p}_+(x,s), \tag{14a}$$

$$s\tilde{p}_-(x,s) - \tfrac{1}{2}\delta(x) = -\partial_x[(f(x) - v_0)\tilde{p}_-(x,s)] + r\tilde{p}_+(x,s) - r\tilde{p}_-(x,s) + T\,\partial_{xx}\tilde{p}_-(x,s), \tag{14b}$$

where $\tilde{p}_\pm(x,s) = \int_0^\infty dt\, e^{-st} p_\pm(x,t)$ denotes the Laplace transforms of $p_\pm(x,t)$. Analogous to the analysis of the steady state in the previous section, the symmetry of the problem, including the initial conditions, implies that Eq. (14) need to be solved only for $x \geqslant 0$, since $\tilde{p}_\pm(-x,s) = \tilde{p}_\mp(x,s)$.

Also analogous to the derivation of the SSD, we define $\tilde{P}_0(x,s) = \tilde{P}(x,s)$ to be the Lapalce transform of the SSD, and further introduce the following quantities:

$$\tilde{P}_0(x,s) = \tilde{p}_+(x,s) + \tilde{p}_-(x,s), \tag{15a}$$

$$\tilde{P}_1(x,s) = \partial_x P_0(x,s), \tag{15b}$$

$$\tilde{D}_0(x,s) = \tilde{p}_+(x,s) - \tilde{p}_-(x,s), \tag{15c}$$

$$\tilde{D}_1(x,s) = \partial_x \tilde{D}_0(x,s), \tag{15d}$$

that satisfy the set of Eqs. (14):

$$\partial_x \begin{pmatrix} \tilde{P}_0 \\ \tilde{P}_1 \\ \tilde{D}_0 \\ \tilde{D}_1 \end{pmatrix} = \underbrace{\begin{pmatrix} 0 & 1 & 0 & 0 \\ \frac{s}{T} & -\frac{b}{T} & 0 & \frac{v_0}{T} \\ 0 & 0 & 0 & 1 \\ 0 & \frac{v_0}{T} & \frac{2r+s}{T} & -\frac{b}{T} \end{pmatrix}}_{M_4} \begin{pmatrix} \tilde{P}_0 \\ \tilde{P}_1 \\ \tilde{D}_0 \\ \tilde{D}_1 \end{pmatrix}. \tag{16}$$

In contrast to Eq. (6), this matrix differential equation cannot be decomposed into smaller matrices. For the matrix M_4, we have

$$\mathrm{tr}\, M_4 = -\frac{2b}{T} < 0, \tag{17a}$$

$$\det M_4 = \frac{s(s+2r)}{T} > 0, \tag{17b}$$

which implies that either all the eigenvalues are negative or two are positive and two are negative. In the limit $s \to 0$ corresponding to large times, the eigenvalues approach their respective values for the SSD; see Sec. II. One of the four eigenvalues approaches zero in the limit $s \to 0$, and the remaining three eigenvalues converge to the eigenvalues of the matrix M_3 in Eq. (6). As one of the eigenvalues of M_3 is positive, this rules out the possibility of all four eigenvalues of the matrix M_4 are negative, leaving us with the only option that two eigenvalues are positive and two are negative. The eigenvalues are obtained from the quartic equation:

$$\lambda^4 + \frac{2b}{T}\lambda^3 + \left[-\frac{v_0^2}{T^2} - \frac{2(s+r)}{T} + \frac{b^2}{T^2} \right]\lambda^2 - \frac{2b(s+r)}{T^2}\lambda + \frac{s(s+2r)}{T^2} = 0. \tag{18}$$

Denoting by $\lambda_1(s) > 0$ and $\lambda_2(s) > 0$ the absolute values of the two negative roots of Eq. (18), the rest of the derivation follows almost identically to the derivation of the SSD in

Sec. II. For $x > 0$, we have

$$\tilde{P}_0(x,s) = \frac{B_1}{\lambda_1}e^{-\lambda_1 x} + \frac{B_2}{\lambda_2}e^{-\lambda_2 x}, \tag{19a}$$

$$\tilde{P}_1(x,s) = -B_1 e^{-\lambda_1 x} - B_2 e^{-\lambda_2 x}, \tag{19b}$$

$$\tilde{D}_0(x,s) = \frac{T}{v_0\lambda_1}\left(\frac{b}{T} - \lambda_1 + \frac{s}{T\lambda_1}\right)B_1 e^{-\lambda_1 x} + \frac{T}{v_0\lambda_2}\left(\frac{b}{T} - \lambda_2 + \frac{s}{T\lambda_2}\right)B_2 e^{-\lambda_2 x} \tag{19c}$$

$$\tilde{D}_1(x,s) = -\frac{T}{v_0}\left(\frac{b}{T} - \lambda_1 + \frac{s}{T\lambda_1}\right)B_1 e^{-\lambda_1 x} + \frac{T}{v_0}\left(\frac{b}{T} - \lambda_2 + \frac{s}{T\lambda_2}\right)B_2 e^{-\lambda_2 x}, \tag{19d}$$

where the s dependence of the eigenvalues, λ_1 and λ_2, and the corresponding coefficients, B_1 and B_2, has been omitted for brevity. The latter are obtained from the condition that $\tilde{D}_0(0,s) = 0$, combined with the normalization of the probability distribution, $\int_{-\infty}^{\infty} dx\, \tilde{P}_0(x,s) = \frac{1}{s}$. These yield that

$$\frac{1}{B_1} = 2s\left(\frac{1}{\lambda_1^2} - \frac{1}{\lambda_1\lambda_2}\frac{\frac{b}{T} - \lambda_1 + \frac{s}{T\lambda_1}}{\frac{b}{T} - \lambda_2 + \frac{s}{T\lambda_2}}\right), \tag{20a}$$

$$\frac{1}{B_2} = 2s\left(\frac{1}{\lambda_2^2} - \frac{1}{\lambda_1\lambda_2}\frac{\frac{b}{T} - \lambda_2 + \frac{s}{T\lambda_2}}{\frac{b}{T} - \lambda_1 + \frac{s}{T\lambda_1}}\right). \tag{20b}$$

Taking into account the symmetry of the problem, the time-dependent distribution in Laplace space reads

$$\tilde{P}(x,s) = \frac{B_1(s)}{\lambda_1(s)}e^{-\lambda_1(s)|x|} + \frac{B_2(s)}{\lambda_2(s)}e^{-\lambda_2(s)|x|}. \tag{21}$$

In the limit $s \to 0$, this distribution approaches the SSD obtained earlier in Eq. (11).

In order to complete the derivation, we need to solve Eq. (18) for the two negative eigenvalues, and perform an inverse Laplace transform to obtain $P(x,t)$ from $\tilde{P}(x,s)$ in Eq. (21). Although Eq. (18) can be solved exactly, for example with MAXIMA, a derivation of a closed-form simple expression for the time-dependent probability distribution are practically impossible to obtain because of the s dependence of $\lambda_i(s)$ and $B_i(s)$ $(i = 1, 2)$. Instead, we will now introduce closed-form approximations for the eigenvalues and the normalization coefficients that capture the correct relaxation behaviors at very small and large times, and verify numerically their accuracy at the intermediate timescales.

IV. RELAXATION TO STEADY STATE

Since the probability distribution relaxes to the steady state at very large times, it follows that for $s \to 0$, $\lambda_i(s) \to \lambda_i(0) \equiv \lambda_i$, where λ_i are the corresponding eigenvalues of the M_3 matrix (6). In the opposite limit $s \to \infty$, we expect the eigenvalues to behave like $\lambda_i(s) \sim \sqrt{s/T}$, which is the asymptotic form in Laplace space characterizing the relaxation behavior of a Brownian particle: $\lambda_{\rm Br}(s) = (b + \sqrt{b^2 + 4sT})/2T \overset{s\to\infty}{\sim} \sqrt{s/T}$, and which implies a similar asymptotic behavior in time regime for $t \to 0$, i.e., Gaussian spreading

$$P(x,t) = \frac{e^{-x^2/4Tt}}{\sqrt{4\pi Tt}} + \cdots. \tag{22}$$

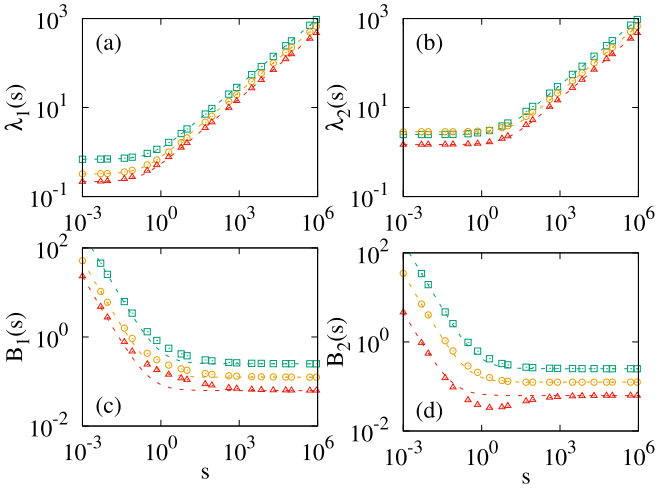

FIG. 3. (a), (b) The dependence of the eigenvalues λ_1 and λ_2, and (c), (d) the coefficients B_1 and B_2, on the Laplace variable s. Symbols indicate the numerically determined values and the dashed lines represent the approximation of Eq. (24). Model parameter values are $r = 1$, $T = 1$, $b = 1$, $v_0 = 1$ (green, squares); $r = 4$, $T = 2$, $b = 1$, $v_0 = 3$ (yellow, circles); $r = 3$, $T = 4$, $b = 1$, $v_0 = 2$ (red, triangles).

The asymptotic similarity with Brownian motion can be understood by noting that at times smaller than the tumbling time, $t \ll r^{-1}$, the particle propagates from the origin subject to action of the thermal and active noises. The latter splits equally between the positive and negative directions at $t = 0$, and has a diminishing probability to flip its direction when $t \to 0$. Thus, the total [active, $\sigma(t)$, and thermal, $\eta(t)$] noise can be written approximately as the sum of two *thermal* white noises, $\eta_\pm(t)$, with constant drift velocities $\langle\eta_\pm(t)\rangle = \pm v_0$ and variances $\langle[\eta_\pm(t') \mp v_0][\eta_\pm(t) \mp v_0]\rangle = 2T\delta(t - t')$:

$$\sigma(t) + \eta(t) \simeq \tfrac{1}{2}\eta_+(t) + \tfrac{1}{2}\eta_-(t) \overset{t\to 0}{\longrightarrow} \eta(t), \tag{23}$$

which manifests the fact that at extremely small times, the active noise is "washed out" by the stronger delta-correlated thermal noise.

With this in mind, we propose the the following approximation for the eigenvalues in Laplace space:

$$\lambda_i(s) \approx \sqrt{s/T + \lambda_i^2}, \quad i = 1, 2, \tag{24}$$

which has the correct asymptotic behavior in the limits $s \to 0$ and $s \to \infty$. Figures 3(a) and 3(b) present the dependence of the $\lambda_i(s)$ $(i = 1, 2)$ on the Laplace variable s. The values of $\lambda_i(s)$, indicated by different symbols of different colors, are obtained by numerically determining the eigenvalues of the matrix M_4 (16) for three different sets of models parameters v_0, r, T, and $b = 1$. As seen in the figures, the agreement between the numerical results and Eq. (24) is nearly perfect over the entire s range, and not only for $s \to 0$. The three sets of model parameters displayed in Fig. 3 correspond to situations in which the active temperature $T_{\rm ac} = v_0^2/2r$ is comparable to the thermal temperature T. Full inspection of the quality of this approximation in cases when one of the temperatures is much larger than the other requires the analysis of a four-

dimensional parameter space, which is beyond the scope of the paper.

Along similar lines, we propose the following form for the coefficients $B_i(s)$ in Eq. (21):

$$B_i(s) \approx \frac{A_i}{s} + \frac{\alpha_i}{T}, \quad i = 1, 2, \tag{25a}$$

$$\alpha_1 = \alpha_2 = \frac{1}{4}. \tag{25b}$$

This form captures the correct asymptotic behaviors in both the small and the large time limits. The first term on the r.h.s. of Eq. (25a) ensures that the SSD is obtained for $t \to \infty$ ($s \to 0$), while the second term on the r.h.s. provides the opposite asymptotic limit, i.e., the coefficient yielding the Gaussian distribution (22) at $t \to 0$ ($s \to \infty$). Note that the coefficients α_i must satisfy $\alpha_1 + \alpha_2 = 1/2$ to ensure the normalization of the distribution function at small times. Based on the numerical results in Figs. 3(c) and 3(d), they are set equal to each other in Eq. (25b), as the results suggest their equality. It implies that, initially, the probability splits equally between the modes, which is in contrast to the steady state at which the contributions of the modes to the total probability are not equal. In other words, the modes are implicitly coupled since probability is transferred between them. Figures 3(c) and 3(d) reveal that Eqs. (25) deviate at the intermediate timescales from the numerically estimated values of $B_i(s)$ which were obtained by substituting the numerical values of the eigenvalues $\lambda_i(s)$ in Eqs. (20). This is not surprising considering that Eqs. (25) are constructed so as to capture only the asymptotic short- and long-time behaviors. In fact, it does not even guarantee that the probability distribution function is normalized to unity except for the two asymptotic limits. In the following subsection, we use the approximations of $\lambda_i(s)$ and $B_i(s)$ to derive an approximate analytical expression for the time-dependent distribution function $P(x, t)$, which is correct asymptotically at small and large time and provides a decent approximation for the relaxation behavior over the entire time domain.

A. Probability distribution

Using Eqs. (24) and (25) in Eq. (21) we write the probability distribution $\tilde{P}(x, s)$ in Laplace space as

$$\tilde{P}_{\rm app}(x, s) = \frac{A_1/s + 1/4T}{\sqrt{s/T + \lambda_1^2}} e^{-\sqrt{s/T+\lambda_1^2}|x|} + \frac{A_2/s + 1/4T}{\sqrt{s/T + \lambda_2^2}} e^{-\sqrt{s/T+\lambda_2^2}|x|}, \tag{26}$$

where the notation "app" serves as a reminder that this form is based on the approximations of $\lambda_i(s)$ and $B_i(s)$. To invert the above Laplace transform, we split the numerator in Eq. (26) into the contributions of the A_i/s and $1/4T$ terms. This leads to the decomposition $\tilde{P}_{\rm app}(x, s) = \tilde{P}_{\rm dec}(x, s) + \tilde{P}_{\rm rel}(x, s)$, where the "decaying" distribution, $\tilde{P}_{\rm dec}(x, s)$, corresponds the sum of terms with prefactor $1/4T$, while the "relaxing" distribution, $\tilde{P}_{\rm rel}(x, s)$, is associated with the sum of terms with prefactor A_i/s. The Laplace inversion of $\tilde{P}_{\rm dec}(x, s)$ results in [62]:

$$P_{\rm dec}(x, t) = \sum_{i=1}^{2} P_{{\rm dec},i}(x, t) = \frac{1}{2\sqrt{4\pi T t}} e^{-\frac{t}{\tau_1} - \frac{x^2}{4Tt}} + \frac{1}{2\sqrt{4\pi T t}} e^{-\frac{t}{\tau_2} - \frac{x^2}{4Tt}}, \tag{27}$$

where

$$\tau_i = \left(\lambda_1^2 T\right)^{-1}, \quad i = 1, 2 \tag{28}$$

are two time constants characterizing the relaxation dynamics of the two Laplace distributions that constitute the SSD, Eq. (11). For the set model parameters $r = 1, T = 1, b = 1, v_0 = 1$, we find $\tau_i = 2.11$ and $\tau_2 = 0.18$, which means that the mode which dominates the SSD in this case relaxes much slower than the other mode. For times $t \ll \min\{\tau_1, \tau_2\}$, with $\min\{,\}$ denoting the minimum of the two arguments, we find $P_{\rm dec}(x, t) \approx \exp[-x^2/4Tt]/\sqrt{4\pi T t} + \cdots$, consistent with Eq. (22).

The term corresponding to A_i/s describes the simultaneous emergence of and relaxation to the steady state. For the Laplace inversion, we use $\mathcal{L}^{-1}[F(s)/s] = \int_0^t \mathcal{L}^{-1}[F(s)](t')dt'$, and obtain

$$P_{\rm rel}(x, t) = \sum_{i=1}^{2} P_{{\rm rel},i}(x, t) = A_1 \int_0^t dt' \sqrt{\frac{T}{\pi t'}} e^{-\frac{t'}{\tau_1} - \frac{x^2}{4Tt'}} + A_2 \int_0^t dt' \sqrt{\frac{T}{\pi t'}} e^{-\frac{t'}{\tau_2} - \frac{x^2}{4Tt'}}. \tag{29}$$

For $t \to \infty$, the two integrals in Eq. (29), represent the Laplace transform of a Gaussian (with $1/\tau_i$ playing the role of the variable s for each relaxation mode), which is the Laplace distribution [62]. Thus,

$$\lim_{t\to\infty} P_{\rm rel}(x, t) = A_1\sqrt{T\tau_1} e^{-|x|/\sqrt{T\tau_1}} + A_2\sqrt{T\tau_2} e^{-|x|/\sqrt{T\tau_2}}, \tag{30}$$

which is the SSD (11) because $\sqrt{T\tau_i} = 1/\lambda_i$ [see Eq. (28)].

Recall that the approximate time-dependent distribution function $P_{\rm app}(x, t) = P_{\rm dec}(x, t) + P_{\rm rel}(x, t)$ is not properly normalized. Explicitly, we have that

$$\mathcal{N}(t) = \int_{-\infty}^{\infty} dx\, P_{\rm app}(x, t) = 1 + \left(\frac{1}{2} - \frac{2A_1}{\lambda_1^2}\right) e^{-t/\tau_1} + \left(\frac{1}{2} - \frac{2A_2}{\lambda_2^2}\right) e^{-t/\tau_2}, \tag{31}$$

and it is easy to verify that $\mathcal{N}(t) \to 1$ in both limits $t \to 0$ and $t \to \infty$. To ensure normalization at all times, we can redefine

$$P_{\rm app}(x, t) = \frac{P_{\rm dec}(x, t) + P_{\rm rel}(x, t)}{\mathcal{N}(t)}, \tag{32}$$

with $P_{\rm dec}(x, t)$, $P_{\rm rel}(x, t)$, and $\mathcal{N}(t)$ given by Eqs. (27), (29), and (31), respectively.

B. Mean square displacement

A quantity of practical interest in context of the dynamics of the RTP is its mean square displacement (MSD):

$$\langle \tilde{x}^2(t) \rangle = \int_{-\infty}^{\infty} dx\, x^2 P(x, t). \tag{33}$$

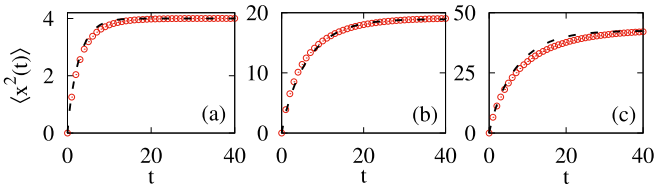

FIG. 4. MSD, $\langle x^2(t)\rangle$, of the RTP evaluated from Langevin dynamics simulations (red circles) vs the predictions of Eq. (34) (black dashed line). Model parameter values are (a) $r = 1,\ T = 1,\ b = 1$, and $v_0 = 1$; (b) $r = 4,\ T = 2,\ b = 1$, and $v_0 = 3$; and (c) $r = 3,\ T = 4,\ b = 1$, and $v_0 = 2$. The black dashed lines show the theoretically estimated MSD [Eq. (34)]. Langevin dynamics simulations were conduced with the Euler integration method with time step $dt = 4 \times 10^{-3}$ and are based on 5×10^7 trajectories. Error bars in the simulation results are smaller than the symbol sizes.

Using $P_{\rm app}(x,t)$ from Eq. (32) in Eq. (33), we obtain

$$\langle x^2_{\rm app}(t)\rangle = \left\{\frac{4A_1}{\lambda_1^2}\left[1-\left(1+\frac{t}{\tau_1}\right)e^{-\frac{t}{\tau_1}}\right]+\frac{t}{\tau_1}e^{-\frac{t}{\tau_1}} + \frac{4A_2}{\lambda_2^2}\left[1-\left(1+\frac{t}{\tau_2}\right)e^{-\frac{t}{\tau_2}}\right]+\frac{t}{\tau_1}e^{-\frac{t}{\tau_2}}\right\} \times\left[1+\left(\frac{1}{2}-\frac{2A_1}{\lambda_1^2}\right)e^{-t/\tau_1}+\left(\frac{1}{2}-\frac{2A_2}{\lambda_2^2}\right)e^{-t/\tau_2}\right]^{-1}. \tag{34}$$

Figure 4 shows Langevin dynamics results for the MSD, $\langle x^2(t)\rangle$, for the three sets of model parameters also displayed in Fig. 3. The results are found in a very good agreement with Eq. (34), which lends credibility to our approximations.

C. Local relaxation time

At small times and to leading order, Eq. (34) reads $\langle x^2(t)\rangle \approx 2Tt$, suggesting that initially the dominant relaxation mechanism is thermal diffusion. This is anticipated considering the asymptotic behavior of $P(x,t)$; see Eq. (22). Furthermore, from the small time limit $t \to 0$ in Eq. (27) for $P_{\rm dec}(x,t)$, we can conclude that thermal Gaussian spreading governs the relaxation to steady state on times $t \lesssim \tau_i$ and on length scales $|x| \lesssim \lambda_i^{-1}$. This spatial region constitutes the "core" of the distribution, where the steady-state probability is concentrated. The same conclusion can be also inferred from $P_{\rm rel}(x,t)$ in Eq. (29), from which we can estimate the fraction of the probability density that has already relaxed to the steady state

$$\Pi_{{\rm rel},i}(t) \equiv \int_{-\infty}^{\infty} P_{{\rm rel},i}(x,t)dx = 2A_i T\tau_i(1-e^{-t/\tau_i}), \tag{35}$$

which approaches saturation exponentially with timescale τ_i.

At larger times, the relaxation dynamics can be inferred from Eq. (29) for $P_{\rm rel}(x,t)$. The integrals in this equation can be evaluated using the saddle-point approximation. Explicitly, we define the variable $0 \leqslant u = t'/t \leqslant 1$ and rewrite

$$P_{{\rm rel},i}(x,t) = A_i\sqrt{\frac{Tt}{\pi}}\int_0^1 du\,\frac{e^{-t\phi(u)}}{\sqrt{u}}, \tag{36}$$

where $\phi(u) = [u/\tau_i + x^2/(4Tt^2u)]$. The maximum contribution to the integral $P_{{\rm rel},i}(x,t)$ comes from the minimum of the function $\phi(u)$, which is at $u_{0,i} = (|x|/t)\sqrt{\tau_i/4T}$ if x and t are such that $u_{0,i} < 1$. If $u_{0,i} \geqslant 1$ then the maximal contribution to the integral comes from the end of the interval, i.e., $u_{0,i} = 1$. Note that the saddle-point approximation is applicable at large times, when the integrand in Eq. (36) is *sharply* peaked. At such large times, the $1/\sqrt{u}$ contribution in Eq. (36) is negligible. With this in mind we find that the saddle-point approximation yields that

(1) The distribution function relaxes to the SSD for $|x| < 2(\sqrt{T/\tau_i})t$: $P_{{\rm rel},i}(x,t) = (A_i/\lambda_i)e^{-\lambda_i|x|}$.

(2) The distribution function takes a Gaussian form for $|x| > (2\sqrt{T/\tau_i})t$:$P_{{\rm rel},i}(x,t) \sim (A_i/\lambda_i)e^{-t/\tau_i}e^{-x^2/4Tt}$.

From (i) we identify a "relaxation front" propagating along the x axis at velocity $v_i^* = 2\sqrt{T/\tau_i}$ [which can also be written $v_i^* = 2T\lambda_i$; see Eq. (28)]. The distribution function relaxes to steady state at points that have been passed by the front ($|x| < v_i^* t$) and decays as a Gaussian at points not yet passed by the front ($|x| > v_i^* t$). Keep in mind that the saddle point approximation is applicable only at times $t \gtrsim \tau_i$ and distances $|x| \gtrsim \lambda_i^{-1}$. In other words, the relaxation front with constant velocity applies only to the "rare" part of the distribution, i.e., the exponential tail of the SSD.

To summarize the discussion on the nature of the relaxation dynamics at small and large times: Defining the coordinate-dependent *local* relaxation time, $t(x)$, as the time at which the distribution function saturates to its steady-state value at distance $|x|$ from the origin, it is suggested that $t(x)$ levels off to a constant for small $|x|$, and increases linearly for large $|x|$. To test these predictions, we propose an operational definition for $t(x)$, as the time at which the relative difference between the distribution function at x and its steady-state value falls below some threshold value ε: $|P(x,t(x)) - P(x)|/P(x) < \varepsilon$. Note that $t(x)$, as operationally defined for computer simulations, is an effective time which is not required to coincide with the value of τ_i in the small $|x|$ regime. Also, $t(x)$ accounts for the combined contribution of the two relaxation modes. However, for the set of parameters used in our simulations ($b = 1,\ r = 1,\ D = 1$ and $T = 1$), one of the modes is significantly more dominant than the other; thus, $t(x)$ should follow the trends emerging from the single mode analysis, i.e., approach a constant value close to the origin and increase linearly away from it. Figure 5(a) shows Langevin dynamics results for $t(x)$ with the relaxation threshold set to $\varepsilon = 0.1$. The small- and large-$|x|$ behaviors are indeed observed in the simulation results. Surprisingly, $t(x)$ does not grow monotonically but features a sudden dip at intermediate values of x, indicating that local relaxation is quickly established at this range. The origin of this distinctive nonmonotonic behavior may be understood from the data for $P(x,t)$ plotted against the SSD, $P(x)$, in Fig. 6 at various times. At small $|x|$, $P(x,t)$ exceeds $P(x)$, which can be ascribed to the outward thermal diffusion of probability from the origin. At large $|x|$, $P(x,t)$ approaches $P(x)$ from below, and the local relaxation is characterized by the relaxation front. The drop in $t(x)$ at the intermediate range can be attributed to the cancellation of these opposing trends. In Fig. 5(b) we plot the local relaxation time of a Brownian particle that starts at the origin and moves in the same confining potential $U(x) = b|x|$ with $b = 1$ at temperature $T = 1$.

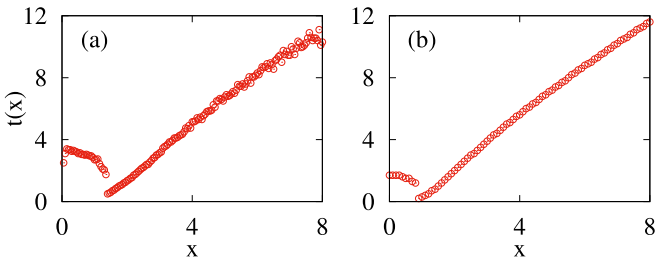

FIG. 5. (a) Local relaxation time, $t(x)$, for the RTP obtained by Langevin dynamics simulations with parameters $b = 1$, $r = 1$, $v_0 = 1$, and $T = 1$. (b) The same for a Brownian particle with $b = 1$ and $T = 1$. The RTP results are obtained from Langevin dynamics simulations, while the Brownian motion results are derived from the exact solution for $P(x, t)$ (see Ref. [63]). Langevin dynamics simulations were conduced with the Euler integration method with time step $dt = 4 \times 10^{-3}$ and are based on 2×10^6 trajectories.

The results for $t(x)$ in Fig. 5(b) are derived directly from the exact solution of $P(x, t)$, which is known [63]. The similarity between the two subfigures is striking, especially in the nearly discontinuous drop at the intermediate timescales.

V. ENTROPY PRODUCTION AT STEADY STATE

The rate of entropy production can be calculated exactly for the model system considered herein. For clarity and to explicitly show the dimensionality of the quantities involved, we reintroduced in what follows the Boltzmann constant, k_B, and the mobility, μ, which were previously set to unity. At steady state, the rate of entropy production of the RTP in a confiding potential is given by (see Sec. 3.2 in [64])

$$\dot{S} = \frac{v_0}{\mu T} \int_{-\infty}^{\infty} [v_0 P(x) - \mu b \, \mathrm{sgn}(x) D_0(x)] dx, \tag{37}$$

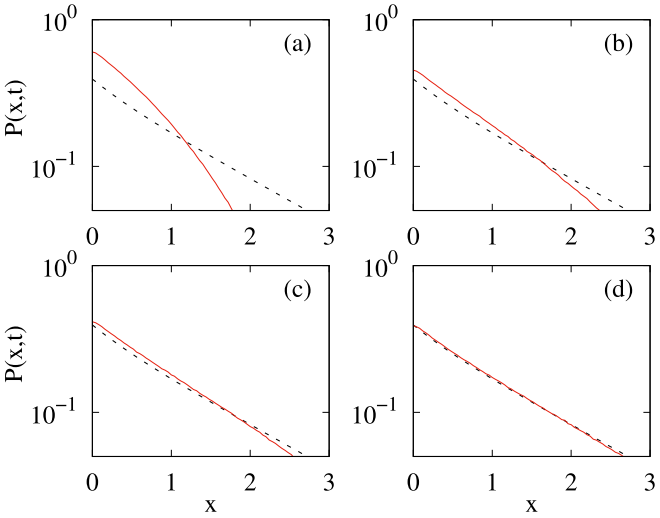

FIG. 6. Probability distribution, $P(x, t)$, of the RTP at times (a) $t = 0.5$, (b) $t = 1.5$, (c) $t = 2.5$, and (d) $t = 4.5$. Red lines, Langevin dynamics simulations; black dashed line, the SSD. Langevin dynamics simulations were conduced with the Euler integration method with time step $dt = 4 \times 10^{-3}$ and are based on 10^6 trajectories.

where $P(x)$ is the SSD (11) and $D_0(x) = p_+(x) - p_-(x)$ is given in Eq. (10). Performing the integrals yields

$$\dot{S} = \frac{v_0^2}{\mu T} - \frac{2\mu b^2}{T} \left\{ \left[1 - \frac{\lambda_1 k_B T}{b} \right] \frac{A_1}{\lambda_1^2} + \left[1 - \frac{\lambda_2 k_B T}{b} \right] \frac{A_2}{\lambda_2^2} \right\}. \tag{38}$$

Denoting the fractional weights of the two modes composing the SSD by $\phi_i = 2A_i/\lambda_i^2$ ($\phi_1 + \phi_2 = 1$), Eq. (38) can be written as

$$\dot{S} = \frac{v_0^2 - \mu^2 b^2}{\mu T} + k_B \mu b^2 \left(\frac{\lambda_1}{b} \phi_1 + \frac{\lambda_2}{b} \phi_2 \right). \tag{39}$$

Equation (39) expresses the rate of entropy production in terms of the partition of the steady-state probability between the modes and their respective correlation lengths λ_i. Defining the effective mode temperatures $k_B T_i = b/\lambda_i$ from the equivalent Boltzmann distributions $\exp(-\lambda_i |x|) = \exp(-b|x|/k_B T_i)$, we have

$$\begin{aligned} \dot{S} &= \frac{v_0^2 - \mu^2 b^2}{\mu T} + \mu b^2 \left(\frac{\phi_1}{T_1} + \frac{\phi_2}{T_2} \right) \\ &= \frac{v_0^2}{\mu T} + \mu b^2 \left(\frac{\phi_1}{T_1} + \frac{\phi_2}{T_2} - \frac{1}{T} \right). \end{aligned} \tag{40}$$

The second equality in (40) suggests that entropy production at steady state consists of two contributions: one associated with the energy required for the generation of the active noise source, and the other related to heat exchange between the thermal bath and the two mode subsystems. Keep in mind that the simple form of the second contribution may be a bit misleading because the temperatures (T_i) and the sizes (ϕ_i) of the two modes depend on all the model parameters, including T and v_0.

In the limit $v_0 \to 0$, $r \to 0$ with a finite active temperature $k_B T_{\mathrm{ac}} = v_0^2/2\mu r$, we have $\phi_1 = \phi_2 = 0.5$, and $T_1 = T_2 = T$ yielding $\dot{S} = 0$ (see Fig. 2). Moreover, the SSD in this case converges to the equilibrium Boltzmann distribution $P(x) \sim \exp[-b|x|/k_B T]$, suggesting that the system approaches the pure thermal limit. Interestingly, the influence of such a weak ($v_0 \to 0$) but persistent ($r \to 0$) telegraphic noise does not fade away when the particle is *not* subject to a confining potential, i.e., for $b = 0$. In free space, the long-time diffusion coefficient is the sum of thermodynamic and active temperatures and is equal to $\mu k_B (T + T_{\mathrm{ac}})$ [65], highlighting the differences between nonequilibrium entropy production in open versus confined systems. In other words, in this limit the configurational temperature defined by the SSD remains the thermal temperature T, while the kinetic temperature defined by the diffusion coefficient and via the Einstein relation is $T + T_{\mathrm{ac}}$.

VI. SUMMARY AND CONCLUSIONS

We study motion of a run and tumble particle in a piecewise linear confining potential in contact with a heat bath. The active noise modifies the natural tendency of a Brownian particle to relax to the equilibrium Boltzmann distribution. We find that the probability distribution $P(x, t)$ of the RTP is described by a mixture of two distributions, both in transient as well as at the steady state. At short times, $P(x, t)$ is a mixture of two Gaussian distributions, while at long times it relaxes to a

mixture of two Laplace distributions. The relaxation towards the steady state $P(x)$ is quite nontrivial. The particle starts at the origin and, thus, the steady state builds from the center outwards, but the local relaxation time $t(x)$ exhibits a distinctive nonmonotonic behavior with a sharp minimum at intermediate length scales. Close to the origin, at the core of the distribution, thermal diffusion dominates the relaxation dynamics, while at the tails it is established at times that grow linearly with $|x|$. The propagation of the relaxation front in the tail of the distribution is governed by exponentially rare stochastic trajectories that exhibit persistent motion in a single direction, with characteristic durations that scale linearly with $|x|$. This relaxation behavior is also observed in the case of pure Brownian motion, i.e., in the absence of active noise. However, the presence of active noise qualitatively alters the distribution, leading to a splitting into two distinct modes. These modes are characterized by effective temperatures, relaxation times, and front propagation velocities, all of which depend in a nontrivial and intricate way on the model parameters, including the thermodynamic temperature of the surrounding heat bath.

The detailed analysis presented in this work is limited to the system in a Markovian setting. This, however, is a sort of an idealization as independence of tumbling times may not always hold in practice, for example, for swimming bacteria [66]. This also brings us within the realm of heterogeneous diffusion processes with inclusion of memory effects [67,68]. We shall explore these non-Markovian effects [58] and related properties in future works. We will also extend our investigations to other forms of confining potentials, including these where the steady state of the pure RTP is defined only over a finite support, and where constant active temperatures T_i that are associated with Botzmann-like distributions are not straightforwardly defined. Finally, it would be also interesting to expand our study to dimensions higher than one. While exact solutions of RTP dynamics are typically hard to obtain in two and three dimensions, in cases where there is spherical symmetry, the SSD may have similar characteristics to the one-dimensional solution because the orientational moves can be mapped onto a one-dimensional model with different statistics of tumbling lengths [27,69].

ACKNOWLEDGMENTS

This work was supported by the Israel Science Foundation (ISF), Grant No. 1258/22. We thank Naftali Smith for useful discussions. R.K.S. thanks the Kreitman Fellowship for financial support and Eli Pollak for discussions about Laplace inversions.

DATA AVAILABILITY

The data that support the findings of this article are openly available [70].

[1] P. Romanczuk, M. Bär, W. Ebeling, B. Lindner, and L. Schimansky-Geier, Active Brownian particles: From individual to collective stochastic dynamics, Eur. Phys. J. Spec. Top. **202**, 1 (2012).

[2] M. C. Marchetti, J.-F. Joanny, S. Ramaswamy, T. B. Liverpool, J. Prost, M. Rao, and R. A. Simha, Hydrodynamics of soft active matter, Rev. Mod. Phys. **85**, 1143 (2013).

[3] S. Ramaswamy, Active matter, J. Stat. Mech. (2017) 054002.

[4] C. Bechinger, R. Di Leonardo, H. Löwen, C. Reichhardt, G. Volpe, and G. Volpe, Active particles in complex and crowded environments, Rev. Mod. Phys. **88**, 045006 (2016).

[5] É. Fodor and M. C. Marchetti, The statistical physics of active matter: From self-catalytic colloids to living cells, Physica A **504**, 106 (2018).

[6] F. Backouche, L. Haviv, D. Groswasser, and A. Bernheim-Groswasser, Active gels: Dynamics of patterning and self-organization, Phys. Biol. **3**, 264 (2006).

[7] D. Mizuno, C. Tardin, C. F. Schmidt, and F. C. MacKintosh, Nonequilibrium mechanics of active cytoskeletal networks, Science **315**, 370 (2007).

[8] T. Toyota, D. A. Head, C. F. Schmidt, and D. Mizuno, Non-Gaussian athermal fluctuations in active gels, Soft Matter **7**, 3234 (2011).

[9] B. Stuhrmann, M. Soares e Silva, M. Depken, F. C. MacKintosh, and G. H. Koenderink, Nonequilibrium fluctuations of a remodeling *in vitro* cytoskeleton, Phys. Rev. E **86**, 020901(R) (2012).

[10] C. Wilhelm, Out-of-equilibrium microrheology inside living cells, Phys. Rev. Lett. **101**, 028101 (2008).

[11] W. W. Ahmed, É. Fodor, and T. Betz, Active cell mechanics: Measurement and theory, Biophysica Acta **1853**, 3083 (2015).

[12] M. E. Cates, Diffusive transport without detailed balance in motile bacteria: Does microbiology need statistical physics? Rep. Prog. Phys. **75**, 042601 (2012).

[13] T. Vicsek, A. Czirók, E. Ben-Jacob, I. Cohen, and O. Shochet, Novel type of phase transition in a system of self-driven particles, Phys. Rev. Lett. **75**, 1226 (1995).

[14] J. Toner, Y. Tu, and S. Ramaswamy, Hydrodynamics and phases of flocks, Ann. Phys. **318**, 170 (2005).

[15] R. Golestanian, T. B. Liverpool, and A. Ajdari, Designing phoretic micro-and nano-swimmers, New J. Phys. **9**, 126 (2007).

[16] S. C. Takatori, R. De Dier, J. Vermant, and J. F. Brady, Acoustic trapping of active matter, Nat. Commun. **7**, 10694 (2016).

[17] O. Dauchot and V. Démery, Dynamics of a self-propelled particle in a harmonic trap, Phys. Rev. Lett. **122**, 068002 (2019).

[18] A. Deblais, T. Barois, T. Guerin, P.-H. Delville, R. Vaudaine, J. S. Lintuvuori, J.-F. Boudet, J.-C. Baret, and H. Kellay, Boundaries control collective dynamics of inertial self-propelled robots, Phys. Rev. Lett. **120**, 188002 (2018).

[19] R. Di Leonardo, L. Angelani, D. Dell'Arciprete, G. Ruocco, V. Iebba, S. Schippa, M. P. Conte, F. Mecarini, F. De Angelis, and E. Di Fabrizio, Bacterial ratchet motors, Proc. Natl. Acad. Sci. USA **107**, 9541 (2010).

[20] A. Sokolov, M. M. Apodaca, B. A. Grzybowski, and I. S. Aranson, Swimming bacteria power microscopic gears, Proc. Natl. Acad. Sci. USA **107**, 969 (2010).

[21] J. Saragosti, V. Calvez, N. Bournaveas, B. Perthame, A. Buguin, and P. Silberzan, Directional persistence of chemotactic bacteria in a traveling concentration wave, Proc. Natl. Acad. Sci. USA **108**, 16235 (2011).

[22] M. Sidortsov, Y. Morgenstern, and A. Be'er, Role of tumbling in bacterial swarming, Phys. Rev. E **96**, 022407 (2017).

[23] J. Taktikos, H. Stark, and V. Zaburdaev, How the motility pattern of bacteria affects their dispersal and chemotaxis, PLoS ONE **8**, e81936 (2013).

[24] M. Goral, E. Clement, T. Darnige, T. Lopez-Leon, and A. Lindner, Frustrated 'run and tumble'of swimming *Escherichia coli* bacteria in nematic liquid crystals, Interface Focus **12**, 20220039 (2022).

[25] A. P. Solon, M. E. Cates, and J. Tailleur, Active Brownian particles and run-and-tumble particles: A comparative study, Eur. Phys. J. Spec. Top. **224**, 1231 (2015).

[26] M. E. Cates and J. Tailleur, When are active Brownian particles and run-and-tumble particles equivalent? Consequences for motility-induced phase separation, Europhys. Lett. **101**, 20010 (2013).

[27] J. Elgeti and G. Gompper, Run-and-tumble dynamics of self-propelled particles in confinement, Europhys. Lett. **109**, 58003 (2015).

[28] B. Ezhilan, R. Alonso-Matilla, and D. Saintillan, On the distribution and swim pressure of run-and-tumble particles in confinement, J. Fluid Mech. **781**, R4 (2015).

[29] L. Angelani, Confined run-and-tumble swimmers in one dimension, J. Phys. A: Math. Theor. **50**, 325601 (2017).

[30] A. Villa-Torrealba, C. Chávez-Raby, P. de Castro, and R. Soto, Run-and-tumble bacteria slowly approaching the diffusive regime, Phys. Rev. E **101**, 062607 (2020).

[31] F. Mori, P. Le Doussal, S. N. Majumdar, and G. Schehr, Universal properties of a run-and-tumble particle in arbitrary dimension, Phys. Rev. E **102**, 042133 (2020).

[32] F. Mori, P. Le Doussal, S. N. Majumdar, and G. Schehr, Universal survival probability for a d-dimensional run-and-tumble particle, Phys. Rev. Lett. **124**, 090603 (2020).

[33] D. Frydel, Generalized run-and-tumble model in 1D geometry for an arbitrary distribution of drift velocities, J. Stat. Mech. (2021) 083220.

[34] L. Angelani, One-dimensional run-and-tumble motions with generic boundary conditions, J. Phys. A: Math. Theor. **56**, 455003 (2023).

[35] J. Masoliver and G. H. Weiss, Finite-velocity diffusion, Eur. J. Phys. **17**, 190 (1996).

[36] J. M. Porra, J. Masoliver, and G. H. Weiss, When the telegrapher's equation furnishes a better approximation to the transport equation than the diffusion approximation, Phys. Rev. E **55**, 7771 (1997).

[37] G. H. Weiss, Some applications of persistent random walks and the telegrapher's equation, Physica A **311**, 381 (2002).

[38] J. Klafter and I. M. Sokolov, *First Steps in Random Walks: From Tools to Applications* (Oxford University Press, Oxford, 2011).

[39] A. Dhar, A. Kundu, S. N. Majumdar, S. Sabhapandit, and G. Schehr, Run-and-tumble particle in one-dimensional confining potentials: Steady-state, relaxation, and first-passage properties, Phys. Rev. E **99**, 032132 (2019).

[40] F. J. Sevilla, A. V. Arzola, and E. P. Cital, Stationary superstatistics distributions of trapped run-and-tumble particles, Phys. Rev. E **99**, 012145 (2019).

[41] P. Le Doussal, S. N. Majumdar, and G. Schehr, Velocity and diffusion constant of an active particle in a one-dimensional force field, Europhys. Lett. **130**, 40002 (2020).

[42] N. R. Smith and O. Farago, Nonequilibrium steady state for harmonically confined active particles, Phys. Rev. E **106**, 054118 (2022).

[43] H. Risken, *The Fokker-Planck Equation: Methods of Solution and Applications* (Springer, Risken, Berlin, 1996).

[44] M. Guéneau, S. N. Majumdar, and G. Schehr, Optimal mean first-passage time of a run-and-tumble particle in a one-dimensional confining potential, Europhys. Lett. **145**, 61002 (2024).

[45] M. Guéneau, S. N. Majumdar, and G. Schehr, Run-and-tumble particle in one-dimensional potentials: Mean first-passage time and applications, Phys. Rev. E **111**, 014144 (2025).

[46] J. Gachelin, A. Rousselet, A. Lindner, and E. Clement, Collective motion in an active suspension of *Escherichia coli* bacteria, New J. Phys. **16**, 025003 (2014).

[47] H. Wioland, E. Lushi, and R. E. Goldstein, Directed collective motion of bacteria under channel confinement, New J. Phys. **18**, 075002 (2016).

[48] G. Tucci, É. Roldán, A. Gambassi, R. Belousov, F. Berger, R. G. Alonso, and A. J. Hudspeth, Modeling active non-Markovian oscillations, Phys. Rev. Lett. **129**, 030603 (2022).

[49] D. Wexler, N. Gov, K. Ø. Rasmussen, and G. Bel, Dynamics and escape of active particles in a harmonic trap, Phys. Rev. Res. **2**, 013003 (2020).

[50] R. Garcia-Millan and G. Pruessner, Run-and-tumble motion in a harmonic potential: Field theory and entropy production, J. Stat. Mech. (2021) 063203.

[51] D. Frydel, Positing the problem of stationary distributions of active particles as third-order differential equation, Phys. Rev. E **106**, 024121 (2022).

[52] A. Arcobi and S. Burov, Continuous approximation of stochastic maps for modeling asymmetric cell division, arXiv:2307.09391.

[53] P. Le Doussal, S. N. Majumdar, and G. Schehr, Stationary nonequilibrium bound state of a pair of run and tumble particles, Phys. Rev. E **104**, 044103 (2021).

[54] N. R. Smith, P. Le Doussal, S. N. Majumdar, and G. Schehr, Exact position distribution of a harmonically confined run-and-tumble particle in two dimensions, Phys. Rev. E **106**, 054133 (2022).

[55] H. K. Barman, A. Nandi, and D. Das, Optimizing search processes in systems with state toggling: Exact condition delimiting the efficacy of stochastic resetting strategy, arXiv:2410.06933.

[56] M. Bier and R. D. Astumian, Matching a diffusive and a kinetic approach for escape over a fluctuating barrier, Phys. Rev. Lett. **71**, 1649 (1993).

[57] F. Ginot, A. Solon, Y. Kafri, C. Ybert, J. Tailleur, and C. Cottin-Bizonne, Sedimentation of self-propelled Janus colloids: Polarization and pressure, New J. Phys. **20**, 115001 (2018).

[58] O. Farago and N. R. Smith, Confined run-and-tumble particles with non-Markovian tumbling statistics, Phys. Rev. E **109**, 044121 (2024).

[59] C. W. Gardiner, *Handbook of Stochastic Methods for Physics, Chemistry and the Natural Sciences*, Springer Series in Synergetics (Springer, Gardiner, Berlin, 1985).

[60] R. W. D. Nickalls, Viete, Descartes and the cubic equation, Math. Gaz. **90**, 203 (2006).

[61] I. J. Zucker, The cubic equation—A new look at the irreducible case, Math. Gaz. **92**, 264 (2008).

[62] F. Oberhettinger and L. Badii, *Tables of Laplace Transforms* (Springer Science & Business Media, Oberhettinger, New York, 2012).

[63] M. Chase, K. Spendier, and V. M. Kenkre, Analysis of confined random walkers with applications to processes occurring in molecular aggregates and immunological systems, J. Phys. Chem. B **120**, 3072 (2016).

[64] M. Paoluzzi, A. Puglisi, and L. Angelani, Entropy production of run-and-tumble particles, Entropy **26**, 443 (2024).

[65] K. Malakar, V. Jemseena, A. Kundu, K. Vijay Kumar, S. Sabhapandit, S. N. Majumdar, S. Redner, and A. Dhar, Steady state, relaxation and first-passage properties of a run-and-tumble particle in one-dimension, J. Stat. Mech. (2018) 043215.

[66] F. Detcheverry, Generalized run-and-turn motions: From bacteria to Lévy walks, Phys. Rev. E **96**, 012415 (2017).

[67] T. Sandev, L. Kocarev, R. Metzler, and A. Chechkin, Stochastic dynamics with multiplicative dichotomic noise: Heterogeneous telegrapher's equation, anomalous crossovers and resetting, Chaos Solits. Fractals **165**, 112878 (2022).

[68] T. Sandev and A. Iomin, Fractional heterogeneous telegraph processes: Interplay between heterogeneity, memory, and stochastic resetting, Phys. Rev. E **110**, 024101 (2024).

[69] N. R. Smith, Nonequilibrium steady state of trapped active particles, Phys. Rev. E **108**, L022602 (2023).

[70] https://bgu365-my.sharepoint.com/:f:/g/personal/ofarago_bgu_ac_il/EnLVWUeQLRlDgs3DTHKIiZEB5_OwPjfJNTwXvrYop3R-vQ?e=ZbnV5l.